Digest Journal of Nanomaterials and Biostructures Vol. 12, No. 3, July - September 2017, p. 689 - 695

MODIFICATION OF STRUCTURAL AND ELECTRICAL PROPERTIES OF ZnO THIN FILMS BY Ni^{2+} IONS IRRADIATION

M. F. KHAN[a*], K. SIRAJ[a], A. SATTAR[b*], H. FAIZ[a], A. USMAN[b], J. RAISANEN[c]

[a]*Laser and Optronics Centre, Department of Physics, University of Engineering and Technology, Lahore 54000, Pakistan.*

[b]*Department of Physics, COMSATS Institute of Information Technology, Lahore 54000, Pakistan.*

[c]*Department of Physics, Division of Materials Physics, University of Helsinki, Helsinki, Finland.*

This work investigates the induced modification in structural, surface and electrical properties of pristine and 700 KeV Ni^{2+} ion irradiated ZnO thin films at different fluences (1×10^{13}, 1×10^{14} and 2×10^{14}, ions/cm^2). The structural properties were studied using X-ray diffraction and it shows that the average crystallite size of ZnO thin films is observed to increase by the ion fluence. The atomic force microscopy (AFM) study shows that the roughness of irradiated thin films decreases which depicted the growth of smaller nano crystalline on the surface of thin films. The electrical resistivity decreases at the fluence of 1×10^{13} ions/cm^2 from pristine value. The resistivity increases by further increases the ion fluence. The modifications of structural, surface and electrical properties are well explained on the basis of annealing effect and oxygen vacancies induced by irradiation. Density functional theory (DFT) calculations are used to simulate the effect of doping of Ni ions in ZnO wurtzite structure. Calculation of band structure and density of states supports the experimentally results of resistivity trend.

(Received April 26, 2017; Accepted July 22, 2017)

Keywords: Ni ion irradiation, thin films, DFT, Simulations, electrical resistivity, AFM

1. Introduction

Zinc Oxide is an n-type semiconductor with wide band gap 3.37 eV and large excitonic binding energy 60 meV [1]. Pure and doped ZnO thin films have been subjected of vast attention due to their significant technological applications such as blue/UV LED's, soler cell, ultra violet nano-lasers, gas sensors, piezoelectric materials, spintronic and optoelectronic devices [2-10].

A variety of techniques have been used for the preparation of ZnO thin films, the properties of grown thin films and interface depends on the deposition process and deposition parameters. These techniques include pulsed laser deposition, magnetron sputtering thermal sputtering, magnetron sputtering, sol gel, chemical bath deposition , Molecular Beam Epitaxy, electro-deposition etc. [11-17]. Out of these used Pulsed laser deposition (PLD) technique to synthesize high quality thin films [18].

Ion irradiation is a unique post deposition technique to modify structural, optical and electrical properties of thin films, when intense interaction of incident ions with the target atoms. Ion irradiation can create new defects and anneal out preexisting defects in the same material [19]. The incorporation of impurities (Co, Ni, Fe, Au, etc.) is key towards controlling the conductivity in ZnO, it has been postulated that the unintentional n-type conductivity in ZnO is caused by the presence of oxygen vacancies or zinc interstitials [20].

ZnO has been extensively studied using computational techniques such as density functional theory to unveil the underlying physics. Both LDA and GGA approximations give

[*]Corresponding authors: asattar@ciitlahore.edu.pk

underestimated results for the band gap of ZnO. The correction can be introduced by using LDA+U method [21]. The ion irradiation of ZnO can lead to both ion implantation and crystal defects such as vacancies. Oxygen vacancies are found to be the lowest energy defect followed by Zn interstitial and Zn on Oxygen site substitution [22]. In the simulation of present work we have discussed the oxygen vacancies and implantation of Ni^{2+} ions in ZnO.

2. Experimental

In this experiment ZnO thin films were fabricated on ultrasonically cleaned glass substrate (10 mm × 10mm ×1mm) by pulsed laser deposition technique. KrF excimer laser (λ = 248 nm, ϕ = 2.5 J/cm^2, N_l = 7500, ν = 10 Hz) was used to ablate the pure ZnO target. The substrate temperature and background oxygen pressure were 300°C and 10^{-2} mbar respectively. The thickness of all the deposited ZnO thin films were 250 ± 10 nm, calculate from spectroscopic ellipsometry technique. The deposited ZnO thin films were irradiated with 700 keV Ni^{2+} ions with fluences 1×10^{13}, 1×10^{14} and 2×10^{14} ions/cm^2 using Pelletron tandem accelerator. Irradiation was carried out at room temperature and high vacuum condition. Using Srim simulation [23] the electronic stopping power of 700 keV Ni ions in ZnO thin films was 61.80 eV/Å, while nuclear stopping power was 94.02 eV/Å. The estimated projected range and lateral straggling were 310 nm and 100 nm respectively. The range of ions was greater than the thickness, therefore most of the ions were stopped in the glass substrate. Modification in crystalline structure is analyzed by X-ray diffractometer (XRD) using Cu K_α 1.5405 Å radiations in 2θ range of 20 to 90°. Surface morphology is studied by atomic force microscope (AFM) in tapping mode. The electrical resistivity estimated by using four point probe technique.

3. Results and discussion

3.1. Structural analysis

Crystallinity of pristine and Ni^{2+} ions irradiated ZnO thin films were investigated by x-ray diffraction (XRD) technique. Fig. 1 depicts that pristine ZnO thin film exhibited a preferential orientation along c-axis with (002) plane at 34.24°. When ZnO thin films were irradiated with 700 keV Ni^{2+} ions indicating that ZnO stayed crystalline, but after irradiation observed a low intensity peak of NiO (220) plane at 62.67°. NiO phase formation showed that the Ni^{2+} ions are incorporated to Zn site during irradiation, which indicated by the variation in 2θ position of ZnO (002) plane. The crystallite size and lattice constant of the (002) plane was calculated using following equations [24-25]:

$$D = \frac{0.9\,\lambda}{\beta\cos\theta} \quad (1)$$

$$\frac{1}{d^2} = \frac{4}{3}\left(\frac{h^2+hk+k^2}{a^2}\right) + \frac{l^2}{c^2} \quad (2)$$

Where λ is the wavelength of X-ray, Θ is the Bragg diffraction angle, β is the observed full width half maximum (FWHM) and dkhl is the crystalline plane distance for indices (hkl) and the value could obtained for XRD pattern.

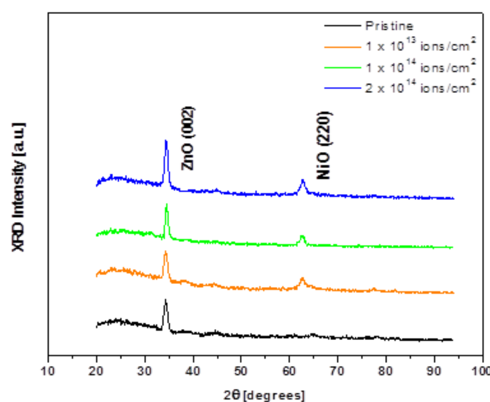

Fig. 1. XRD spectra of pristine, and Ni^{+2} ions irradiated ZnO thin films

The crystallography parameters calculated from XRD spectra are given in table 1, it is evident from the table that all irradiated ZnO thin films have shift towards higher 2θ value and reduced the lattice constant as compared to pristine ZnO thin film indicating the presence of compressive stresses. The crystallite size increases from 9.4 nm (pristine) to 14.3 nm at the high fluence, i.e. 2×10^{14} ions/cm^2. The increase in crystallite size with increasing ion fluence indicating improved crystallinity of ZnO thin films. This could be attributed to reduction in strain by annealing effect due the imparted energy of the incoming ions according to thermal spike model and result in the improved crystallinity of ZnO thin films [26].

Table 1. Different parameters of pristine and Ni^{+2} irradiated ZnO thin films at different ion fluences.

Sr. No.	Ions fluences (ions/cm^2)	2Θ (degree)	FWHM (degree)	Crystallite Size D(nm)= $\frac{k\lambda}{\beta\cos\theta}$	Lattice parameter (c) Å	Resistivity (Ω-cm)
1	Pristine	34.24	0.88	09.4	5.228	3.84×10^{-1}
2	1×10^{13}	34.28	0.74	11.2	5.220	4.47×10^{-4}
3	1×10^{14}	34.76	0.69	12.0	5.179	3.01×10^{-2}
4	2×10^{14}	34.40	0.58	14.3	5.220c	4.42×10^{-1}

3.2. Surface morphology

Surface topography of pristine and Ni^{2+} ions irradiated ZnO thin films were studied by atomic force microscope (AFM) in tapping mode. Fig. 2, shows the 2-D and 3-D surface profile (scan area 2 µm × 2 µm) of pristine and Ni^{2+} ions irradiated ZnO thin films. The root mean square (rms) roughness of pristine film is about 5.25 nm due to the inhomogeneous distribution of grains on the surface. The roughness was decreased after ion irradiations from pristine value i.e. 4.96 nm, 4.35 nm and 4.07 nm at the fluence of 1×10^{13}, 1×10^{14}, 2×10^{14} ions/cm^2 respectively. The decrease in roughness of ion irradiated ZnO thin films were attributed to the formation of smaller sized nano-crystallites, grain growth and better filling of pores upon radiation due to increase of local annealing effect. The appearance of the nano-crysallites structures also signifies the improvement in crystallinity of thin films as indicated by XRD results.

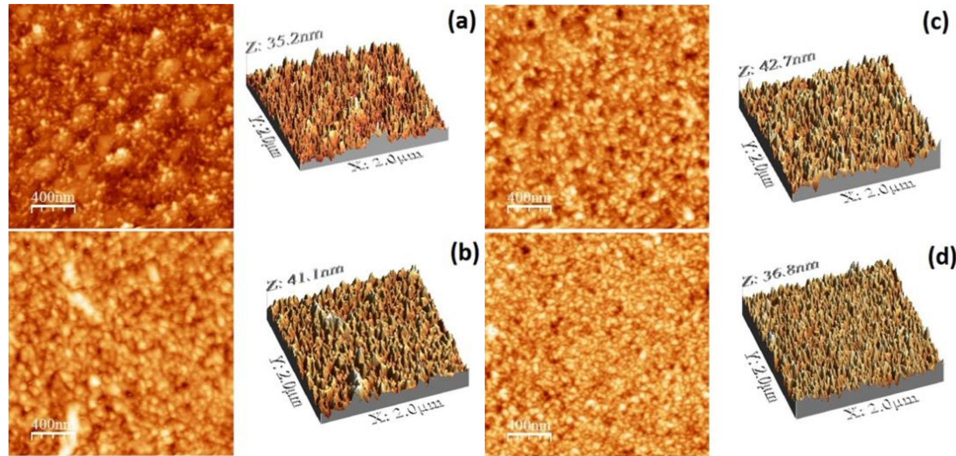

Fig. 2.Atomic force microscopy graphs (2-D and 3-D) of pristine and Ni^{+2} ions irradiated ZnO thin films at different ion fluence. (a) Pristine, (b) 1×10^{13} ions /cm^2, (c) 1×10^{14} ions /cm^2, (d) 2×10^{14} ions /cm^2

3.3. Electrical Resistivity

Electrical resistivity measurements were carried out for pristine and Ni^{2+} ions irradiated ZnO thin films using four-point probe method. The electrical resistivity of thin films was calculated by substituting the observed data in equation [27]

$$\rho = \left(\frac{\pi}{ln2}\right)\left(\frac{V}{I}\right)t \tag{3}$$

Where the term in first pretenses is the correction factor, I is the current applied between two outer probes, V is the voltage drop across inner probes, and t is the thickness of thin film, calculated values of electrical resistivity shown in table 1.

Fig. 3 (main panel) shows the electrical resistivity of ZnO thin films decrease form 3.84×10^{-1} Ω-cm (pristine) to 4.47×10^{-4} Ω-cm (at the flow fluence of 1×10^{13} ions /cm^2). The possible reason for decrease in electrical resistivity is that the incoming ions produce some structural defects, creation of oxygen vacancies and zinc interstitial in thin film [28]. Further increase in ions fluence (i.e. 1×10^{14} and 2×10^{14}ions /cm^2) the electrical resistivity increases to 3.01×10^{-2} Ω-cm and 4.42×10^{-1} Ω-cm. The appropriate reason is that, the incident ions energy produced localized annealing effect at high fluence along with the Ni^{2+} ions substitution in the ZnO matrix. This results in improved crystallinity of thin films and hence it increase electrical resistivity of ZnO thin films as observed in reference [29].

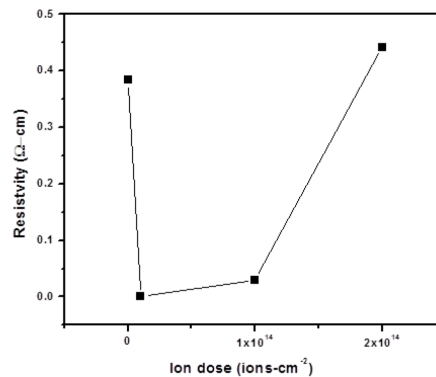

Fig. 3. Variation of electrical resistivity of Ni^{+2} ions irradiated ZnO thin films at different fluences

3.4. Simulations

DFT simulations for pristine ZnO, ZnO with Oxygen vacancy and ZnO irradiated with Ni ions were performed to probe the physics behind the variation observed in the experiments. ATK DFT package was used for the simulations. Fig. 4. Shows the structures of the super cell used for above mentioned three cases. The band structures and density of states were calculated using DFT for wurtzite ZnO with ideal structure, with oxygen vacancy and with Zn substitute with Ni. Generalized Gradient Approximation (GGA+U) was used for all the simulations with 4 k points in each direction a, b and c. An onsite Hubbard potential was fixed at 10eV for 3d electrons of Zn atoms to achieve band gaps similar to those of the experimental values. The Ni ion bombardment can easily knock out the host atoms producing point defects (vacancies) in the structure of pure ZnO. Also due to very similar atomic radii Ni can also act as a substitute atom to substitute the host Zn.

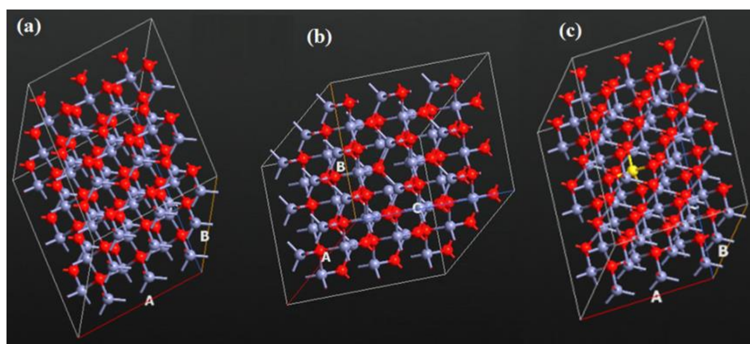

Fig. 4. Supercell used for the DFT calculations. (a) Pure ZnO wurtzite structure, (b) ZnO wurtzite structure with Oxygen vacancy, (c) ZnO wurtzite structure with Zn atom substituted by Ni atoms.

The sudden decreases in the resistivity shown in the fig. 3 could be explained by the formation oxygen vacancies and Ni ion substitution of Zn. As it can be clearly seen in the fig 5 (a) and (b) pure ZnO has a wide band gap. Due to the ion bombardment vacancy and substitution defects are produced in pristine structure of ZnO. Fig 5 (c) and (e) shows that new energy levels are introduced due to Ni ion implantation and oxygen vacancies. In case of Ni doping two new levels just below conduction band minima at 1.6 eV and 0.9 eV above fermi level appear whereas for oxygen vacancy a new level appears around fermi lever. As shown in the fig. 5 (d) and (f) peaks corresponding to these two levels can be seen in the density of states. These states provide transmission channels for the electron conductance causing significant reduction of resistivity consistent with four probe results shown in the fig. 3. Electronic levels in case of Ni doping are located close to conduction band minima (CBM) and act as shallow donors. Resistivity is decreased due to highly delocalized d electrons of Ni atoms injecting free electrons in the conduction band of ZnO. At lower ion fluences the decrease in resistivity is due to impurity Ni ions is much greater compared to the increase in resistivity due to the competing factor of annealing due to thermal energy transfer. On the other had ZnO thin films does contain a lot of oxygen vacancies inherently due to the mobile nature of oxygen ions. These oxygen vacancies provide a band with significant density of state just around the fermi level (Fig. 5. (f)). Due to the high fluence Ni ions impart more and more energies to the film initiating annealing like process due to increase in the temperature. Due to this the crystallite size of the film increases as shown in the Table 1, causing decrease in defects and oxygen vacancies and hence increase in the resistivity of the film. Increase in the resistivity at the fluence $1x10^{14}$ ion/$cm^2$and higher the increase in crystallinity is much more important compared to its competing effect of Ni^{2+} substituting which tries to decrease resistivity.

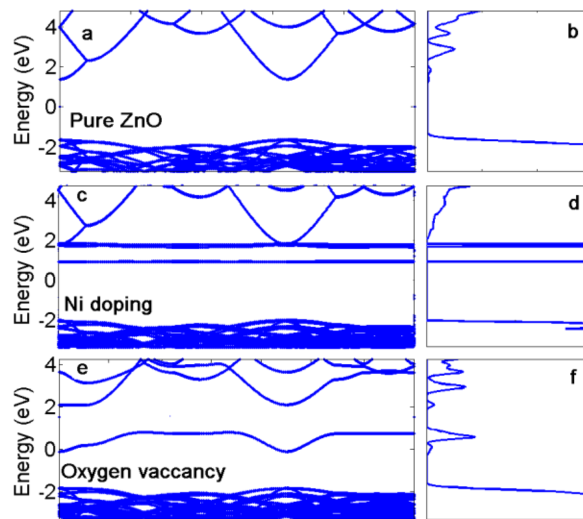

Fig. 5. Band structure (left panels) (a,c,e) and density of states (right panels) (b,d,f) of ZnO thin films. (a,b) pure ZnO, (c,d) ZnO with oxygen vacancy and (e,f) ZnO with Ni^{+2} irradiation

4. Conclusions

We have investigated modification of structural, surface and electrical properties of pristine and Ni^{2+} ions irradiated ZnO thin films. We have observed after irradiation the crystallinity improved, roughness decreases and electrical resistivity increases of ZnO thin films. The irradiation induced local annealing effect and oxygen vacancies and doping of incoming ions in thin films. These experimental results are consistent with the result found using DFT. The resistivity of ZnO decreases exponentially due to the Ni ion where, after initial decrease, resistivity increases due to annealing effect.

Acknowledgment

Authors are thanks to Dr. Hamid Latif, FCCU Lahore Pakistan for providing the facility of computational lab and software for the simulations.

References

[1] M. Peruzzi, J. D. Pedaring, D. B. Bauerle, W. Schwinger, F. Schaffler, Appl. Phys. A **79**, 187 (2014).
[2] S. Kumar, R. Kumar, D. P. Singh, Appl. Surf. Sci. **255**, 8014 (2009).
[3] A. C. Galca, M. Secu, A. Vlad, J. D. Pedaring, Thin Solid Films **518**, 4603 (2010).
[4] A. Vlad, S. Yakumin, E. Klombofer, V. Kolstovska, L. Muresan, A. Sonnleitnew, Thin Solid Films **518**, 1350 (2009).
[5] V. Kumar, R. G. Singh, L. P. Punohit, F. Singh, Advan.Mater. Lett. **4**, 423 (2013).
[6] R. Siddheswaran, M. Netrvalova, J.Savkova, P. Novak, J. Ocenasek, P. S. J. Kovas, J. R. Jayavel, J. Alloy & Comp. **636**, 85 (2015).
[7] A. Kumar, J. B. M. Krishna, D. Dar, S. Keshri, Appl. Surf. Sci. **258**, 2237 (2012).
[8] A. Zhang, Q. H. Li, L. Q. Shi, H. S. Cheng, J. Z. Wang, Nucl. Instrum. Meth. In Phys. Res. B **266**, 4891 (2008).
[9] J.C. Fan, K.M. Sreekanth, Z. Xie, S.L. Chang, K.V. Rao, Proc. in Mater. Sci. **58,** 874 (2013).
[10] S. J. Pearton, D. P. Norton, K. Ip, Y. W. Heo, T. Steiner, Prog. Mater. Sci. **50**, 293 (2005).
[11] W. Prellier, A. Fouchet, Ch. Simon, B. Mercey, Mater. Sci. Engg. B **109**, 192 (2004).

[12] Angadi, R. Kumar, D. H. Park, J. W. Choi, W. K. Choi, Nucl. Instrum. Meth. in Phys. Res. B **272**, 305 (2012).
[13] N. Ehrmann, R. R. Koch, Thin Solid Films **519**, 1475(2010).
[14] M. Subramamanian, M. Tanemura, T. Hihara, V. Ganesan, T. Soga, T. Jimbo, Chem. Phys. Lett. **487**, 97(2010).
[15] M. Cagler, Y. Caglar, S. Aksoy, S. Ilican, Appl. Surf. Sci. **256**, 4966 (2010).
[16] W. Zhiguang, Z. Hang, W. K. Farg, S. Jianrong, Y. Cunferg, S. Tielong, M. Yizhum, P. Lilong, Z. Yabin, Nucl. Instrum. Meth. in Phys. Res. B **269**, 837(2011).
[17] P. M. R. Kumar, C. S. Kartha, K. P. Vijayakumar, F. Singh, D. K. Avasthi, Rad. Eff. Def. in Solids **163**, 635 (2008).
[18] F. K. Shan, Y. S. Yu, Thin Solid Films **435**, 174 (2003).
[19] P. M. R. Kumar, C. S. Kartha, K. P. Vijayakumar, T. Abe, Y. Kashiwaba, G. S. Okram, M. Kumar, S. Kumar, J. of Appl. Phys. **97**, 13509 (2005).
[20] A. Janotti, C. G. V. de Walle, Rep. Prog. Phys. **72**, 126501(2009).
[21] T. R. Paudeland, W. R. L. Lambrecht, Phys. Rev. B **77**, 205202 (2008).
[22] A. Janotti, C. G. Van de Walle, Phys. Rev. B **76**, 165202 (2007).
[23] J. F. Ziegler, M. D. Ziegler, J. P. Biersack, Nucl. Instr. Meth. Phys. Res. B **268**, 1818 (2010).
[24] Y. R. Zhang, J. Wan, Y. U. Ke, J. Hazard. Mater. **177**, 750(2010).
[25] Z. Han, L. Liao, Y. Wu, H. Pan, S. Shen, J. Chen, J. Hazard. Mater. **217**, 100(2012).
[26] M. Fiaz Khan, K. Siraj, M.S. Anwar, M. Irshad, J. Hussain, H. Faiz, S. Majeed, M. Dosmailov, J. Patek, J. D. Pedarnig, M. S. Rafique, S. Naseem. Nucl. Instrum. Meth. in Phys. Res. B. **368**, 45 (2016).
[27] M. Caglar, Y. Caglar, S. Aksoy and S. Ilican, Appl. Surf. Sci. **256**, 4966 (2010).
[28] P. M. R. Kumar, C. S. Kartha, K. P. Vijaykumar, Journal of App. Phys. **97**, 0136509(2005).
[29] Y. Kumar, M. H. Zaldivar, S. F. Olive-Mendez, F. Singh, X. Mathew, V. Agarwal, Nanoscale Res. Lett. **7**, 366 (2012).